npj | genomic medicine

Article

Published in partnership with CEGMR, King Abdulaziz University

https://doi.org/10.1038/s41525-025-00518-z

Rapid generation of a *sdhb* loss-of-function zebrafish model for secreting pheochromocytomas and paragangliomas

S. Parisien-La Salle[1], F. Nobilleau[2,3], A. da Silva Babinet[2], J. Lamontagne[2], M. Labrecque[2], B. Rampal[2,3], C. Mas[2,3], M. Liao[2], V. A. Barragan Torres[4], G. Corbeil[2], L. Chatel-Chaix[4], M. Dona[5], M. Tétreault[2,3], I. Bourdeau[1,6] ✉ & É. Samarut[2,3,6] ✉

Genotype plays a central role in the comprehensive management of pheochromocytomas and paragangliomas, highlighting the critical need for specific in vivo genetic models. Yet, animal models fall short of fully recapitulating the biological complexity of these tumours. We generated first-generation loss-of-function zebrafish models for *sdhb*, a canonical PPGL-associated gene, using CRISPR/Cas9. *Sdhb*-CRISPants exhibit increased heart rates, reduced swimming activity and premature death. In whole fish extracts, normetanephrine (NM), metanephrine (MN), and dopamine (DA) levels were about three times higher in *sdhb* CRISPants than in control larvae. In the bathing medium, NM and MN were also significantly elevated, along with 3-MT. Complementary metabolic and transcriptomic profiling revealed that *sdhb* CRISPants exhibit a clear signature of Complex II dysfunction and upregulation of genes involved in the hypoxia response, angiogenesis, stress response, and glycolysis. Our work validates the relevance of CRISPant zebrafish models to study the pathogenicity of PPGL-causing genetic variants in vivo.

Pheochromocytomas (PHEOs) and paragangliomas (PGLs) (PPGLs) are rare tumors originating from tissues that arise from the embryonic neural crest[1]. PHEOs are located in the adrenal medulla, and PGLs are along the sympathetic and parasympathetic ganglia chains[2]. These tumors can be non-secretory (normal plasma and/or urinary catecholamines) or secretory (plasma and/or urinary catecholamine levels above the upper limit of normal)[3]. PPGLs are the most hereditary tumors in adults[4] with predisposing germline pathogenic variants found in around 40% of cases[5]. Over 20 susceptibility genes are described to date, divided into three clusters. Tumors in the pseudohypoxic cluster 1 are associated with a noradrenergic biochemical phenotype and necessitate close monitoring due to the risk of metastasis and recurrence[6]. Tumors in the kinase signaling-related cluster 2 exhibit an adrenergic phenotype characterized by significant rises in metanephrine levels (MN)[7]. Currently, the clinical characteristics of patients with Wnt signaling-related cluster 3 tumors is less known, but aggressive behavior appears probable[8,9].

With the recent advancements in genetics within the field of PPGLs, genotype has become central to the medical and clinical management of these tumors[5,8]. Firstly, the genotype can impact prognosis and follow-up. Pathogenic variants in specific susceptibility genes, like *SDHB* (*Succinate Dehydrogenase Complex Iron Sulfur Subunit B*), are linked to a poorer prognosis with an increased risk of metastatic or recurrent disease[10,11]. The recurrence rate for PPGLs is ~6.5–17.4%, varying according to the implicated gene[12–14]. Expert consensus recommends that follow-up intensity should be adjusted based on genotype[4,5,8]. Secondly, identifying a germline pathogenic variant enables the presymptomatic screening of family members of an index case[15]. Presymptomatic detection enables the longitudinal monitoring of patients over time, allowing for the identification of disease earlier and reducing the mortality and morbidity associated with PPGLs, particularly in the context of mutated *SDHB* PPGLs[16]. However, when germline and somatic mutations are considered, approximately 30% of PPGLs remain without an identified genetic cause[8]. This gap highlights the need to identify novel genetic variants, which may be uncovered using next-generation sequencing approaches. However, as new PPGL-associated genetic variants are identified, their prevalence is low, and their pathogenicity remains elusive. Indeed, the functional characterization of putative genetic variants associated with PPGL has been

[1]Division of Endocrinology, Department of Medicine, Centre Hospitalier de l'Université de Montréal (CHUM), Montreal, QC, Canada. [2]University of Montréal Hospital Research Center (CRCHUM), Montreal, QC, Canada. [3]Department of Neuroscience, Université de Montréal, Montréal, QC, Canada. [4]Centre Armand-Frappier Santé Biotechnologie, Institut National de la Recherche Scientifique, Laval, QC, Canada. [5]Department of Internal Medicine, Radboud University Medical Center, Nijmegen, the Netherlands. [6]These authors contributed equally: I. Bourdeau, É. Samarut. ✉e-mail: Isabelle.bourdeau@umontreal.ca; eric.samarut@umontreal.ca

limited by the lack of relevant in vivo models combining quantifiable clinically relevant phenotypes (i.e., measurable catecholamine hypersecretion), speed and ease of use (e.g. genetic accessibility and speed of development)[17]. Therefore, there is a need to establish a streamlined process for assessing the pathogenicity of new PPGL susceptibility genes.

SDHB pathogenic variants are among the most frequently identified germline variants in PPGLs and confer an aggressive phenotype with a higher incidence of metastatic disease (up to 46.6%)[18,19]. The *SDHB* gene encodes a subunit of the succinate dehydrogenase (SDH) enzyme, also known as Complex II of the mitochondrial electron transport chain[20]. This enzyme is responsible for converting succinate into fumarate within the Krebs cycle[8]. This gene is included in "cluster 1 A" of PPGL susceptibility genes, which, when mutated, disrupts the Krebs cycle and leads to impaired mitochondrial oxidative phosphorylation, succinate accumulation, and HIF-α stabilization[8]. In *SDHB*-related tumorigenesis, a heterozygous germline mutation is followed by a somatic second hit, such as loss of heterozygosity, leading to biallelic inactivation[21]. This results in accelerated protein degradation, reducing the levels of mutant SDHB protein and leading to insufficient function[22].

Recently, Dona et al. described an *SDHB* mutated zebrafish model that recapitulated some features of PPGLs, such as defects in energy metabolism and swimming behavior, decreased mitochondrial complex 2 activity and succinate accumulation[23]. This was the first evidence that zebrafish can be used as a relevant in vivo proxy for modeling PPGL physiopathology. However, this study relied on a stable CRISPR-engineered zebrafish strain, which requires at least 12–18 months to establish. This timeline does not align with the need for a quick functional assessment of genetic variants associated with PPGLs in vivo. Recently, the same team showed that *SDHB* ± adult fish (note that homozygotes do not reach adulthood) showed only a mild phenotype related to the clinical presentation of PPGLs[24]. This suggests that while these models may enhance our general understanding of underlying mechanisms, they are not well-suited for rapidly assessing the pathogenicity of genetic variants of interest.

In this project, we provide a proof of concept for the rapid in vivo functional characterization of PPGL loss-of-function genetic models. These CRISPant models can be generated and analyzed within a week and are, therefore, compatible with translational precision medicine endeavors.

Results

Sdhb-CRISPant zebrafish depict robust SDHB loss-of-function and associated phenotypes

To efficiently invalidate *SDHB* expression and function in zebrafish embryos, we took advantage of a recently proven F0-knockout mutagenesis approach using CRISPR/Cas9 to generate *SDHB* loss-of-function zebrafish larvae (so-called CRISPants[25]). This approach enables the assessment of phenotypic and biochemical assays in a mutant genetic background of interest within days following microinjection (Fig. 1A). We designed and microinjected one-cell-stage embryos with a CRISPR cocktail targeting the *SDHB* gene at the exons 3, 4, and 5 levels (Fig. 1B). The potency of each guide RNA (gRNA) was assessed by High-Resolution Melting (HRM) analysis (Fig. 1C). The reduction in *sdhb* expression was evaluated at 5 dpf at both the transcriptomic and protein levels using RT-qPCR and western blot, respectively (Fig. 1D–F). Notably, the control groups consisted of embryos microinjected with mRNA encoding the Cas9 endonuclease, but without any gRNAs; these are referred to as "Cas9" in our figures. To validate the relevance of our *sdhb*-CRISPant model, we confirmed several phenotypes previously described in a stable *SDHB*-mutant zebrafish strain[23]. Particularly, we showed that *sdhb*-CRISPant larvae do not survive past 13 dpf (< 50% survival rate reached at 8 dpf, Fig. 1G) and depict a significantly reduced motor activity, especially during light periods, during which Cas9 controls show increased swimming movements (Fig. 1H). Finally, we also confirmed that the *sdhb*-CRISPant larvae exhibit a significantly increased heart rate compared to Cas9 controls (Fig. 1I, J). Altogether, these results confirm the potency of the F0-CRISPant approach to rapidly and efficiently disrupt *sdhb* protein levels and function in vivo.

sdhb-CRISPant zebrafish larvae showed elevated secretion of free catecholamines and MMN

With this new *SDHB*-CRISPant genetic model in our hands, we sought to measure the levels of free catecholamines (e.g., dopamine, norepinephrine and epinephrine) and free MN (e.g., 3-methoxytyramine or 3-MT, normetanephrine (NM) and MN) in larvae lysates and their bathing medium compared to Cas9-controls (Fig. 2A, B). This approach is physiologically relevant, as zebrafish larvae excrete catecholamines and other metabolites into the surrounding medium via the pronephric kidney and cloaca at this stage[26,27]. We found that the levels of NM and MN were three times higher in *sdhb*-CRISPants (NM: 3.69, $p < 0.0001$, MN: 3.35, $p < 0.0001$) compared to control larvae. Interestingly, 3-MT displayed similar levels between both groups. Dopamine (DA) levels were also elevated in *sdhb* larvae compared to Cas9 (2.9, $p < 0.0001$). However, norepinephrine (NE) and epinephrine (E) were lower in *sdhb* mutants compared to Cas9 control larvae (0.81, $p = 0.017$; 0.51, $p < 0.0001$) (Fig. 2C). When we checked the level of these hormones in the fish bathing medium, we also observed that the level of NM, MN, and to a lower extent 3-MT were significantly increased (NM: 4.32, $p < 0.0001$; MN: 9.4, $p < 0.0001$ 3-MT: 1.5, $p = 0.0076$) compared to the bathing medium of Cas9-controls (Fig. 2D). There was no statistical difference for DA and NE in the bathing medium of *sdhb*-CRISPants compared to controls. Of note, the levels of epinephrine were at or below the lower detection limit in most samples for the former and in some samples for the latter (*n.d* in Fig. 2D). Altogether, our data show that *sdhb*-CRISPant larvae display hormonal hypersecretion, which is relevant to *sdhb*-associated PPGLs.

Catecholamine and MN levels are reliable biochemical readouts of different genetic PPGLs

We first wanted to validate the specificity of this hormonal hypersecretion by showing that it cannot be attributed to a nonspecific general physiological distress (i.e., premature death or weakened physiology). To do so, we showed that catecholamine and MN levels are not increased in an independent genetic model. We used the *scn1lab*-mutant genetic model, an ortholog of the human *SCN1A* gene, whose loss of function is associated with epileptic encephalopathy and is characterized by premature death and general physiological distress in zebrafish[28]. In these mutants (*scn1lab*$^{-/-}$), we noted no increase in the levels of free catecholamines and MN, either in larval lysates or in the ambient bath. Instead, the levels of these hormones were significantly reduced in the mutants compared to their siblings (Fig. S1A). More importantly, this confirms that the hormonal hypersecretion observed in our *sdhb*-CRISPant model is specific and cannot be attributed to general physiological distress.

We also wanted to validate the specificity of these significant changes by showing that they cannot be attributed to a nonspecific general metabolic distress caused by the disturbance of the Krebs cycle, as is the case for mutations in PPGL cluster 1[20]. To do so, we generated F0-CRISPRant zebrafish targeting another PPGL canonical gene (*NF1*). This gene belongs to a different genetic cluster (cluster 2) associated with PPGL pathogenesis, which does not affect the integrity of the Krebs cycle but rather kinase signaling[8]. The zebrafish's genome encompasses two paralogous genes (*nf1a* and *nf1b*) orthologous to the human *NF1* gene. Thus, we designed and validated six specific gRNAs (three against each paralog) targeting these genes in zebrafish (Fig. S1B). Notably, we found a significant increase in the level of all free catecholamines (DA: 1.95, $p = 0.0245$; NE:1.47, $p < 0.0001$; E: 1.54, $p < 0.0001$) and all free MN (3-MT: 2.94, $p < 0.0001$; NM 3.86, $p < 0.0001$; MN 4.4, $p < 0.0001$) in *nf1*-CRISPant larvae extracts compared to Cas9-controls (Fig. 2E). Importantly, it is worth noting that the elevation of norepinephrine and epinephrine in *nf1*-CRISPant compared to *sdhb*-CRISPant (Fig. S1C, D) is relevant to an adrenergic phenotype, which is a hallmark of PPGL cluster 2 mutations[8]. Consistently, the level of secreted catecholamines and MN in the bathing medium of *nf1*-CRISPants was also found elevated compared to Cas9-controls (Note that the levels of DA and E were below the detection threshold in this assay, Fig. 2F and S1D). Altogether, these data confirm that the biochemical quantification of free catecholamines and MN from whole larvae lysate and bathing medium is a specific readout of PPGL.

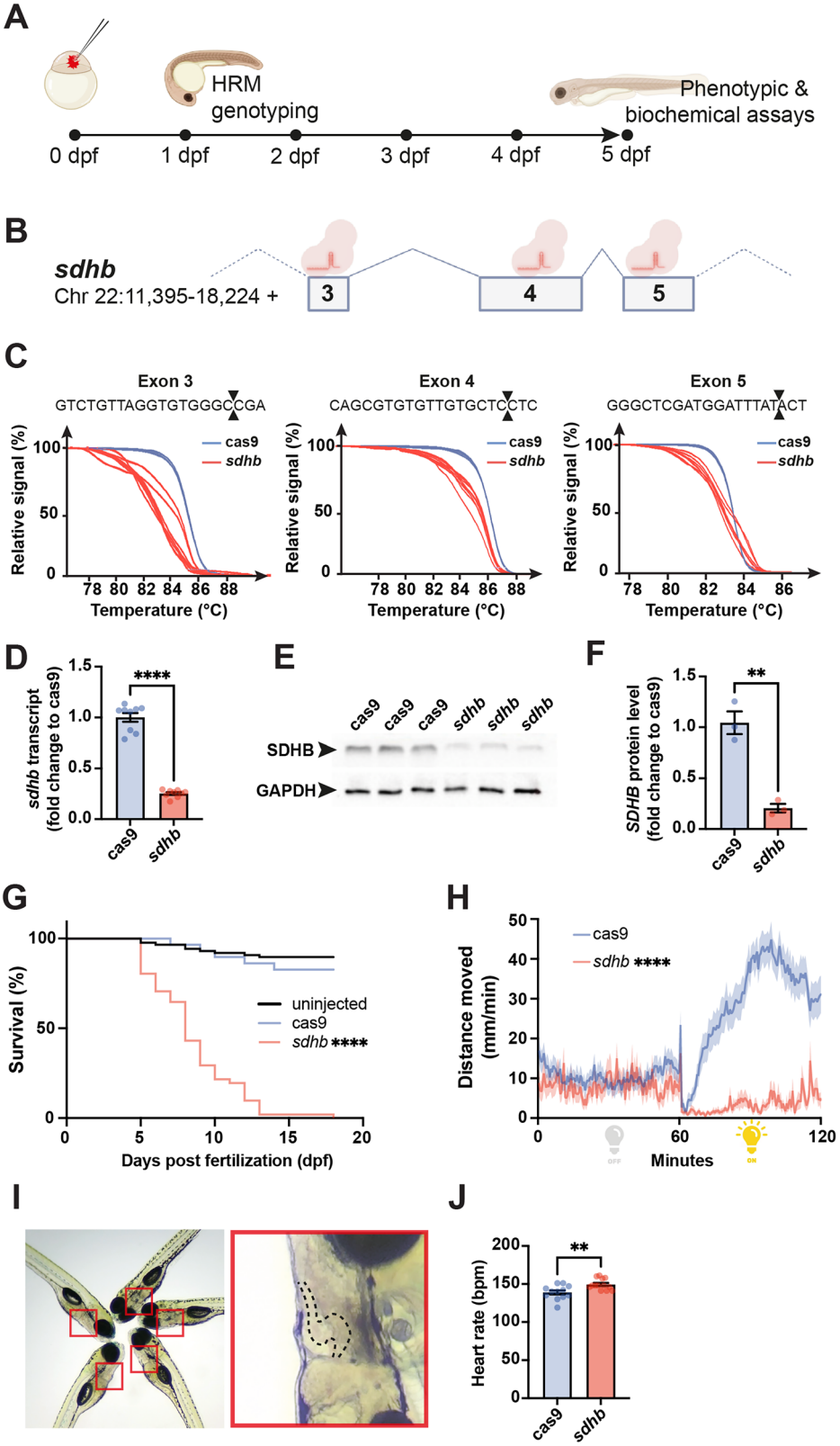

Fig. 1 | F0-injected *sdhb*-CRISPant zebrafish larvae display SDHB-associated phenotypes. **A** Timeline representation of our CRISPant approach starting with the microinjection of a gene-specific (i.e., *sdhb*) CRISPR/Cas9 mix in single-cell embryos, followed by High-Resolution Melting (HRM) genotyping from 1-day post-fertilization (dpf). Phenotypic and biochemical readouts can be acquired only few days following injection. **B** The genetic landscape of the zebrafish *sdhb* gene encompassing targeted exons 3, 4 and 5. **C** The mutagenic power of the injected CRISPR/Cas9 mix is validated by HRM comparing Cas9-injected embryos as controls in which only mRNA encoding CAS9 was microinjected (no gene-specific guide RNAs). **D, E, F** The level of *sdhb* expression is reduced in *sdhb* CRISPants both at the transcriptomic and protein levels as assessed by qRT-PCR (D) and western blot (E, F). (**G**) Survival of *sdhb* CRISPants ($n = 51$) is compared to Cas9-injected controls ($n = 29$) and uninjected larvae ($n = 87$) over 18 days. **H** The distance swam, binned per 30 s, is recorded for sdhb CRISPants ($n = 32$) and Cas9-injected controls ($n = 32$) during 60 min dark and 60 min light periods. **I, J** Representative setup and results of heart rate quantification in 5 dpf larvae (sdhb CRISPants, $n = 13$; Cas9-injected, $n = 12$). **I** Left: larvae mounted laterally in 3% methylcellulose for simultaneous video acquisition (~5 larvae per trial). Red boxes indicate individual larvae analyzed. Right: magnified view of one larva with the heart region outlined (dashed line), corresponding to the area used for automatic beat detection by DanioScope™ software. No anesthetic was used during acquisition. **J** Heart rate was quantified and compared using an unpaired t-test with two-tailed *p*-value calculation: ** *p-value < 0.01;* **** *p-value < 0.0001*. Icons in (**A**) and (**B**) are created in BioRender. Samarut, E. (2025) https://BioRender.com/xk8wiuf.

Sdhb-CRISPant zebrafish larvae display broad metabolic perturbations beyond Krebs metabolites

We next sought to dig into the metabolic perturbations caused by *sdhb* loss-of-function, particularly among Krebs cycle metabolites and related metabolic pathways (Fig. 3A). In whole-larvae lysates, we found a significant increase in the levels of several Krebs cycle intermediates in *sdhb*-CRISPrant compared to Cas9 Controls (Fig. 3E–J). Notably, the levels of acetyl-CoA (1.586 $p = 0.002$; Fig. 3E), citrate-isocitrate (*sdhb*: 2.402 $p = 0.0008$; Fig. 3F) and succinate (*sdhb*: 21.78 $p < 0.0001$; Fig. 3H) were higher in *sdhb* CRISPants than in Cas9-control larvae. This is consistent with the impaired enzymatic activity of SDHB, which converts succinate to fumarate (Fig. 3A). We also looked the levels of glycolysis intermediates and showed that while

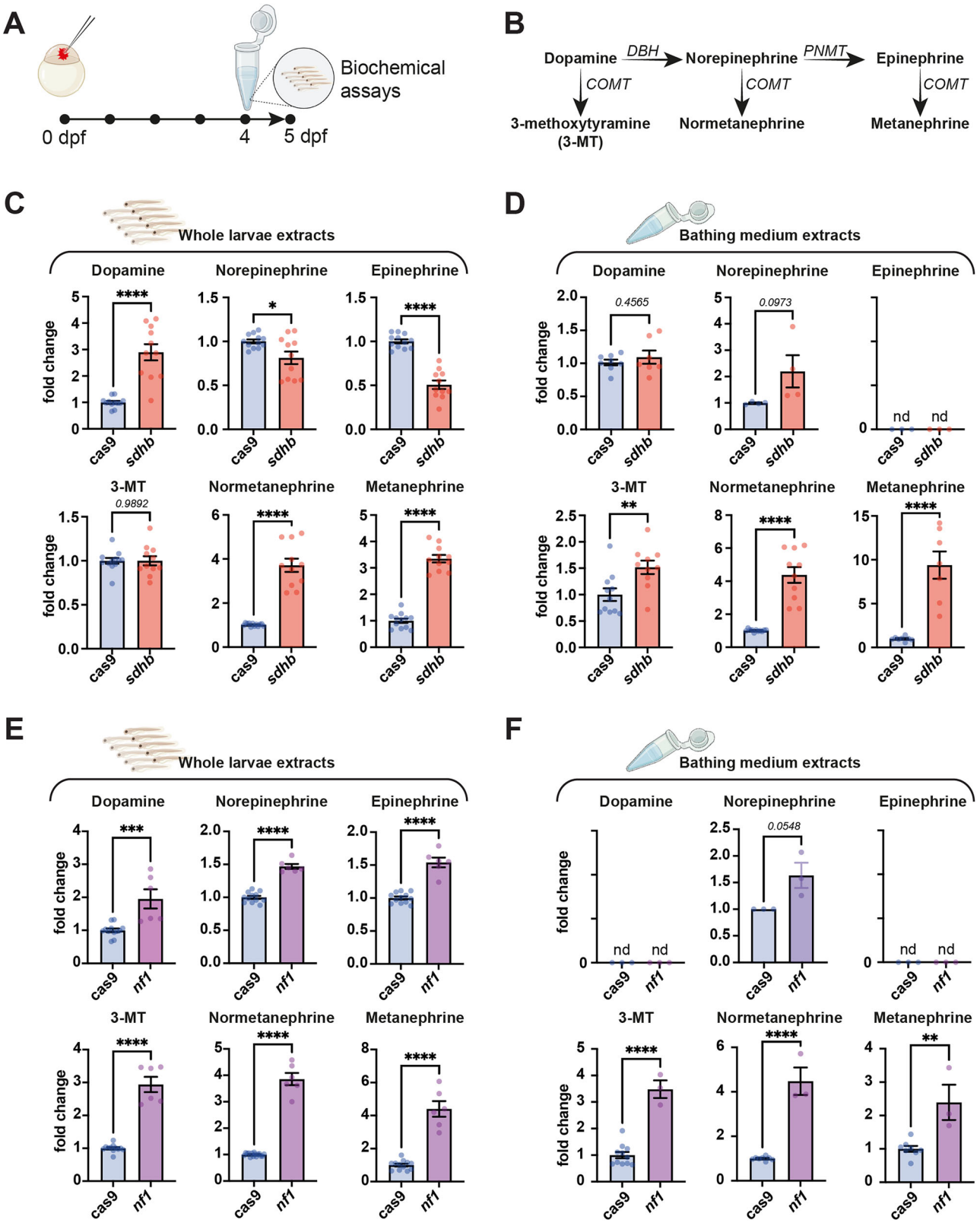

Fig. 2 | Catecholamine and metanephrine levels are affected in PPGL CRISPant zebrafish models. A Individual embryos are microinjected at the one-cell stage and larvae are pooled at 4 dpf overnight. Catecholamines and metanephrines levels were assessed on day 5 from whole larvae lysates and bathing medium. **B** Metabolic path of catecholamines and metanephrine synthesis. Enzymes are italicized (DBH: Dopamine beta-hydroxylase, PNMT: Phenylethanolamine N-Methyltransferase, COMT: Catechol-O-methyltransferase). **C,D** Catecholamines and metanephrines levels in *sdhb* CRISPants ($n \geq 6$ pools of 10 larvae) compared to Cas9-injected controls ($n \geq 6$ pools of 10 larvae) (whole larvae, (**C**) and bathing medium (**D**)). **E,F** Catecholamines and metanephrines levels in *nf1* CRISPants (whole larvae, (**E**) and bathing medium (**F**). Of note, the levels of NE were below the detection limit in Cas9-control samples, and a subjective basal value was used to calculate the NE fold-change increase in *nf1*-CRISPant larvae. Unpaired t-test with two-tailed *p*-value calculation: * *p-value* < 0.05; ** *p-value* < 0.01; *** *p-value* < 0.001; **** *p-value* < 0.0001. Icons are created in BioRender. Samarut, E. (2025) https://BioRender.com/xk8wiuf.

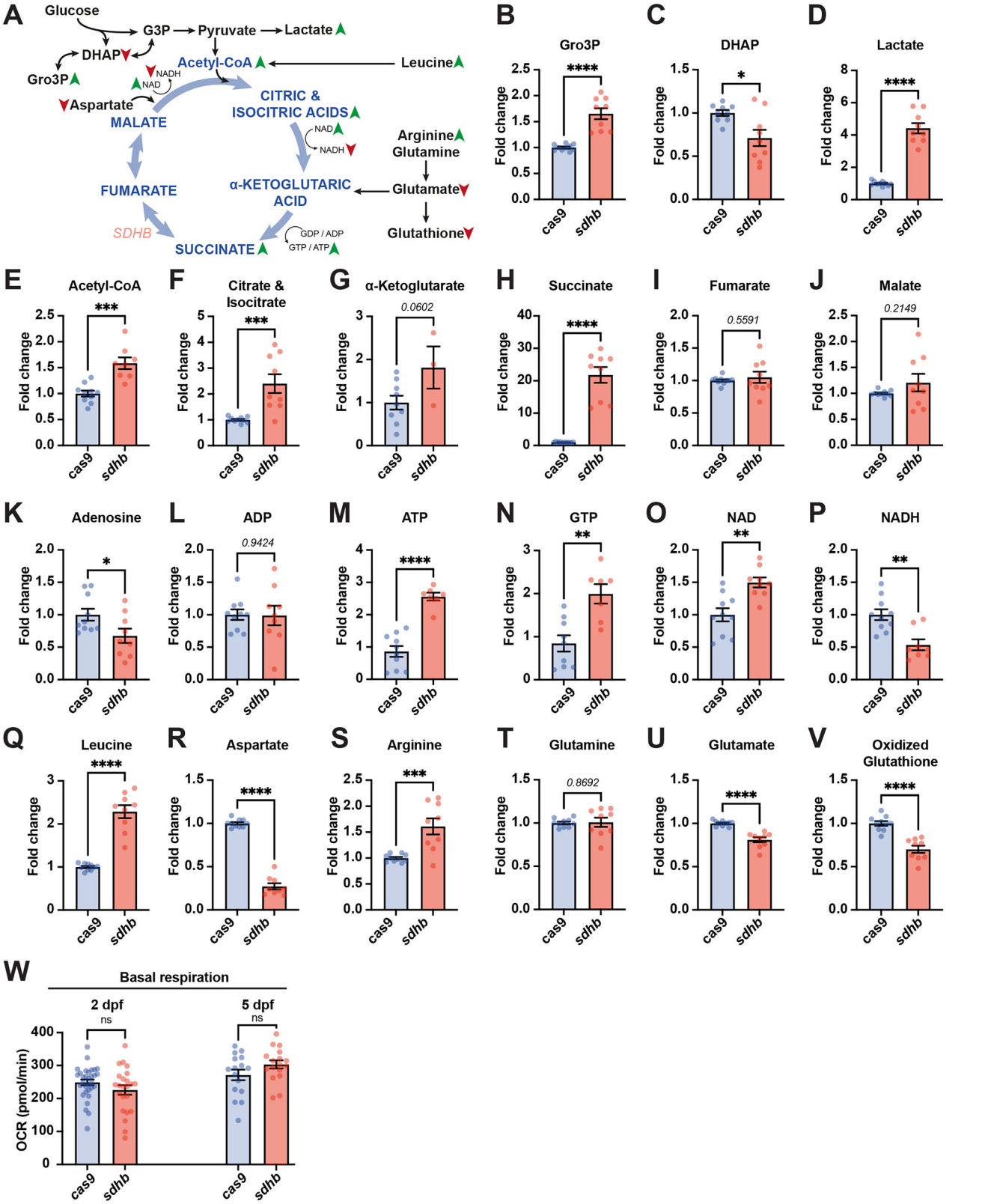

Fig. 3 | *sdhb* CRISPants depict broad metabolic pertubations. A Schematic of Krebs cycle intermediates (in blue) and other metabolites from related pathways (in black) which have been assayed from whole 5 dpf larvae lysates. The changes observed in *sdhb* CRISPants are indicated with arrowheads (green: increase; red: reduction). **B–V** Individual metabolite quantified from whole *sdhb*-CRISPant larvae (pools of 10; $n = 9$ pools of 10) to Cas9-injected control larvae ($n = 10$ pools of 10). **W** Oxygen consumption rate (OCR) was measured in whole Cas9-injected control and *sdhb*-CRISPant larvae at 2 and 5 days post-fertilization (dpf) using a Seahorse XFe96 analyzer. Unpaired t-test with two-tailed *p*-value calculation: * *p-value* < 0.05; ** *p-value* < 0.01; *** *p-value* < 0.001; **** *p-value* < 0.0001.

the levels of glycerol-3-phosphate (Gro3P) (1.652, $p < 0.0001$; Fig. 3B) and lactate (4.421 $p < 0.0001$; Fig. 3D) were significantly increased in *sdhb* CRISPants, the level of DHAP (dihydroxyacetone phosphate) was significantly reduced (0.71, $p = 0.0112$; Fig. 3C). We quantified the levels of various dinucleotides and nucleotides central to bioenergetics (Fig. 3A, K–P). We found that *sdhb*-CRISPant larvae displayed higher levels of ATP (2.560, $p < 0.0001$; Fig. 3M), GTP (1.996, $p = 0.0014$; Fig. 3N) and NAD^+ (1.498, $p = 0.0013$; Fig. 3O) but lower levels of NADH (0.536, $p = 0.0013$) compared to Cas9-control larvae. This suggests significant reprogramming of mitochondrial energy production. Finally, we quantified the levels of several amino acids and other metabolites linked to Krebs cycle and redox regulation (Fig. 3A, Q–V). Interestingly, we noted a significant increase in the levels of leucine (2.287 $p < 0.000\ 1$; Fig. 3Q) and arginine (1.610 $p = 0.0007$; Fig. 3S) in *sdhb*-CRISPant larvae compared to Cas9-controls. Conversely, the levels of aspartate (0.2722 $p < 0.0001$; Fig. 3R), glutamate (0.8111 $p < 0.0001$; Fig. 3U) and oxidized glutathione (*sdhb*: 0.7011 $p < 0.0001$; Fig. 3V) were significantly lower in *sdhb* CRISPants than in *Cas9*-control larvae.

Given that *SDHB* encodes a core subunit of mitochondrial complex II, which links the Krebs cycle to the electron transport chain (ETC), we investigated whether its disruption impairs mitochondrial respiration. To this end, we measured the basal oxygen consumption rate (OCR) in *sdhb* CRISPant zebrafish embryos and larvae using a Seahorse XFe96 analyzer. Surprisingly, OCR was not significantly different from control embryos at either 2 or 5 dpf (Fig. 3W). This unexpected preservation of mitochondrial respiration despite *sdhb* deficiency suggests the activation of compensatory metabolic mechanisms to sustain oxidative phosphorylation. Altogether, while these data confirm the expected changes in the levels of glycolytic and Krebs cycle intermediates associated with the impairment of SDHB activity (i.e., succinate and lactate increase), they also broaden the scope of the metabolic perturbations caused by *sdhb* loss-of-function and indicate that basal mitochondrial respiration is unaffected.

Sdhb loss-of-function leads to broad transcriptomic changes in zebrafish sdhb-CRISPants

Finally, we sought to profile the transcriptional changes caused by *sdhb* loss-of-function in vivo. To do so, we extracted RNAs from whole 5-dpf larvae and sequenced their transcriptome using Next-Generation Sequencing (Fig. 4A). Upon differential gene expression (DEG) analysis, we identified 443 upregulated genes and 326 downregulated genes (filtered by a 5% adjusted *p*-value and log2 Fold Change ≥ 1) in *sdhb* CRISPants compared to Cas9-controls (Fig. 4B and Supplementary Data 1). We built a heat-map plotting the more significant negative DEG correlations between Cas9-control and *sdhb*-CRISPant samples. This map highlights *sdhb* as strongly underexpressed in the mutant situation (Fig. 4C). Conversely, hypoxia response genes (*hif1al* and *igfbp1a)*, angiogenesis gene (*angptl4*), stress response genes (*fkbp5* and *hsd11b2*) and glycolysis gene (*pfkfb4b*) were all upregulated in the mutant condition (Fig. 4C). These expression changes of relevant DEGs (i.e. *hif1al*) were confirmed by RTqPCR on independent biological samples (Fig. 4D–I). We also found that other subunits of the SDH complex, enzymes of the Krebs cycle or mitochondrial biogenesis markers (i.e. PGC1-alpha) showed no significant transcriptional changes (Fig. S2A). Moreover, we examined the differential expression of genes involved in the mitochondrial electron transport chain (ETC) and found that only *sdhb* met our differential expression threshold (log2FC > 1) in *sdhb* CRISPants. Four additional ETC-related genes showed mild but statistically significant regulation: *cox4i2* and *atp1b1a* were moderately upregulated, while *sdhaf2* and *ndufaf3* were slightly downregulated (Supplementary Data 2). These modest changes may reflect localized or adaptive responses to the loss of SDHB. However, the vast majority of ETC components, including structural subunits of complexes I to V, remained transcriptionally unchanged, which is consistent with the preserved oxygen consumption rate (OCR) observed in *sdhb*-deficient larvae (Fig. 3W).

Finally, using DAVID resources[29], we conducted a KEGG pathway enrichment analysis with the DEG list, which included genes that met the criteria of p value ≤ 0.05 and log2 Fold Change ≥ 1, encompassing both upregulated and downregulated genes (Fig. 4J). Our analysis revealed several significantly enriched KEGG pathways in our *sdhb*-CRISPant samples, DNA replication, cell cycle and Metabolic Pathways (Fig. 4J and Supplementary Data 3). These data are consistent with the function of the *SDHB* gene in both the mitochondrial respiratory chain and several main metabolic processes via the Krebs cycle.

Discussion

Genotype constitutes a pivotal factor in the comprehensive management of PPGLs, emphasizing the need to establish genetically engineered biological in vivo models to elucidate underlying pathogenic mechanisms and therapeutic targets. Although it models biallelic *sdhb* loss, our in vivo CRISPant design reflects the fully inactivated state found in tumor tissue[21]. In this study, we present the first published instances of elevated catecholamines/MN in a *sdhb* mutant zebrafish model.

Our *sdhb* CRISPant zebrafish model faithfully recapitulates key features of SDHB-related PPGLs and offers a rapid and scalable in vivo system for functional assessment. This is evidenced by the strong elevation of NM and MN in both whole fish extracts and bathing media, as well as increased dopamine (DA) levels. The excess of NM and MN reached 3–4-fold in tissue and 5–9-fold in the medium. These biochemical alterations are in line with previous descriptions in *sdhb-KO* zebrafish models[23] and provide a phenotypic indication of disease-related catecholamine overproduction. Notably, heart rate was also elevated, suggesting a functional effect of catecholamine excess.

The specificity of the catecholamine profile further validates the relevance of our model. When targeting *nf1*, a PPGL-related gene from a different molecular cluster (Kinase signaling cluster 2 for *nf1* vs. pseudohypoxic signaling cluster 1 for *sdhb*), larvae exhibited an adrenergic profile characterized by elevated NE/E levels[8], while this was absent in *sdhb* CRISPants. This divergence supports the genotype–phenotype specificity of catecholamine dosage in our in vivo models and reinforces the notion that systemic gene disruption in CRISPants reflects localized endocrine effects, particularly at the level of the interrenal gland.

Importantly, this catecholamine elevation cannot be attributed to stress, general weakness, or shortened lifespan. Using the *scn1lab* mutant zebrafish model of Dravet syndrome[28] as a disease control, we observed that these mutants displayed reduced levels of catecholamines/MN despite severe physiological impairment. This strengthens the argument that the catecholamine signature in *sdhb* CRISPants is specific and not a secondary effect of systemic illness.

Beyond catecholamine secretion, our model also replicates other *SDHB*-related clinical features. *Sdhb* CRISPants exhibited impaired mobility, consistent with the hypotonia and muscle dysfunction reported in germline biallelic *SDHB*-deficient patients[30]. This phenotype, although non-tumoral, provides an additional functional endpoint relevant to human disease and suggests broader systemic implications of SDHB loss.

At the metabolic level, our findings point to significant mitochondrial reprogramming in response to SDHB loss. As expected, succinate levels were markedly elevated in *sdhb* larva[31], a hallmark of *SDHx* deficiency observed in patients and associated with malignancy. Our analysis also revealed increased NAD +, reduced NADH, and elevated ATP levels, indicating enhanced NADH oxidation, likely via compensatory complex I activity[32,33]. These adaptations were further reflected by altered levels of lactate (increased), glutamate (decreased), and aspartate (depleted), consistent with a shift toward glycolytic metabolism and anaplerotic support via glutaminolysis[34]. Despite this profound metabolic remodeling, OCR measurements showed no significant decrease, suggesting that mitochondrial respiration is preserved in vivo, likely through these compensatory mechanisms. This was also observed in *C. elegans sdhb-1* mutants, where basal oxygen consumption was comparable to controls. However, these mutants failed to increase respiration in response to a mitochondrial uncoupling agent (FCCP), indicating a loss of spare respiratory capacity and revealing underlying mitochondrial dysfunction[35].

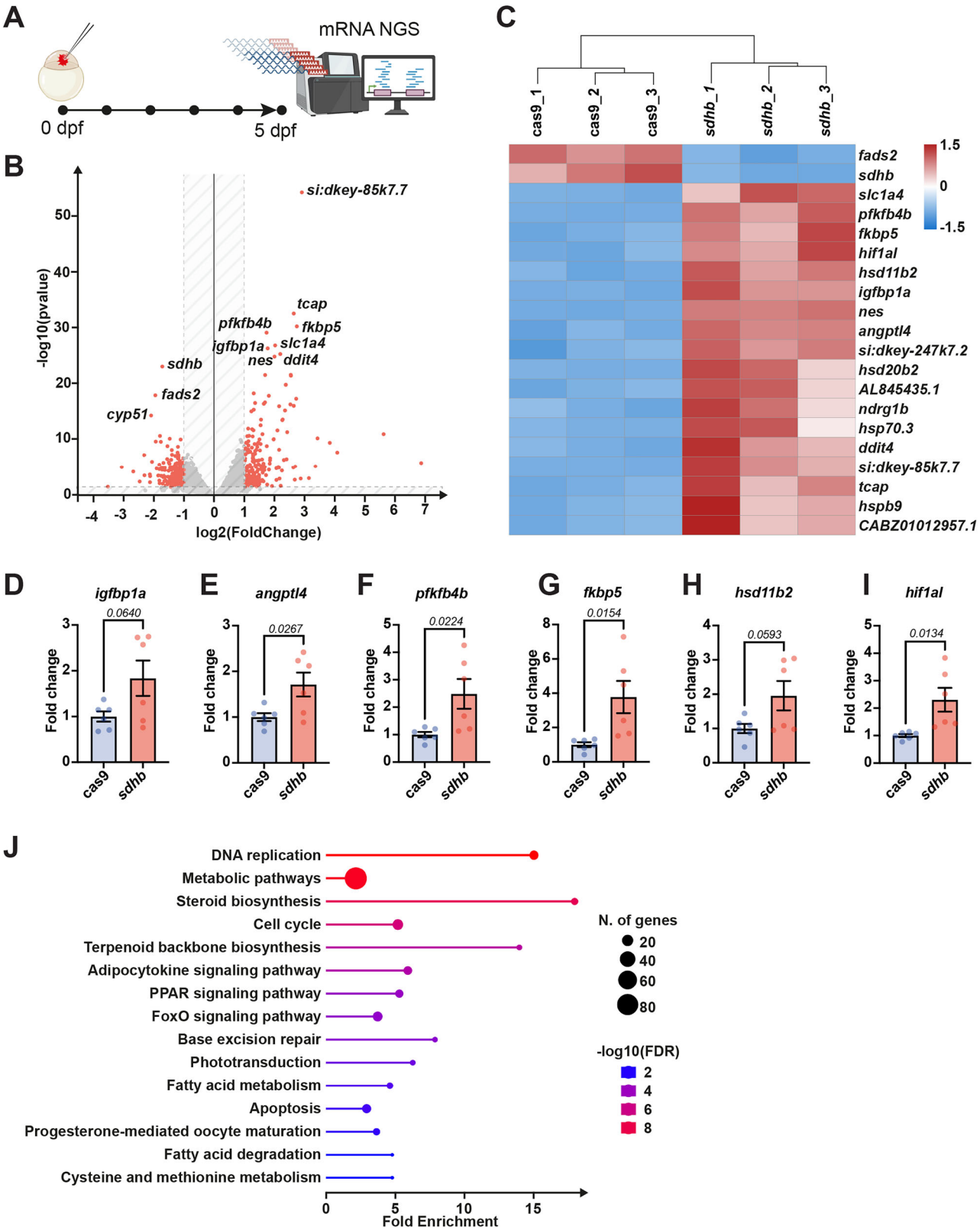

Fig. 4 | Transcriptomic changes in *sdhb* CRISPants. A Experimental timeline from one-cell stage embryo microinjection to whole larvae mRNA extraction at 5 dpf for RNA-sequencing. **B** Volcano plot with differentially expressed genes (DEGs) in red (filtered with a value < 0.05 and an absolute log2FoldChange > 1). The full list of DEGs is available in Supplementary Data 1. **C** Heatmap representing the top 20 DEGs between *sdhb*-CRISPant samples (*sdhb_1, sdhb_2, sdhb_3*) and Cas9 controls (cas9_1, cas9_2, cas9_3). **D–I** qRT-PCR validation of changes in the expression of relevant genes between *sdhb*-CRISPant ($n = 6$ pools of 10 larvae) and Cas9-injected control ($n = 6$ pools of 10 larvae) at 5 dpf. **J** Lollipop plot of top 15 significantly enriched KEGG pathways clustered from *sdhb* vs *cas9* DEGs. The complete list of enriched KEGG pathways is available in Supplementary Data 2. Icons in panel A are created in BioRender. Samarut, E. (2025) https://BioRender.com/xk8wiuf.

Although *SDHB* pathogenic variants are classically associated with PPGLs, they and other PPGL-related genes are often broadly expressed and implicated in fundamental metabolic pathways. Systemic phenotypes observed in our model, including motility defects and metabolic dysfunction, may thus reveal tissue-independent consequences of gene loss and support the use of zebrafish for broader variant modeling.

Transcriptomic profiling supports this interpretation. While *sdhb* was strongly downregulated, confirming CRISPR efficiency, most ETC-related genes remained unchanged, including those of complexes I–V. Only *atp1b1a* and *cox4i2* were modestly upregulated. The latter, a hypoxia-inducible isoform, is consistent with HIF pathway activation. Furthermore, genes involved in glycolysis (*pfkfb4b*), amino acid transport (*slc1a4*, *slc3a2b*), and pyruvate/lactate shuttling (*slc16a6b*) were all upregulated, providing transcriptional evidence of metabolic rewiring. We also observed induction of HIF target genes related to hypoxia (*hif1al*, *igfbp1a*), angiogenesis (*angptl4*), and stress (*fkbp5*, *hsd11b2*)[36]. These changes are in line with succinate-mediated inhibition of prolyl hydroxylases and stabilization of HIF-α[37]. This pattern is consistent with other *SDHB*-deficient cell and animal models[35,38].

Altogether, the combination of succinate accumulation, HIF-*α* stabilization, altered redox status, and transcriptional upregulation of compensatory metabolic genes provides a coherent picture of energy adaptation caused by *sdhb* loss-of-function. These features not only validate the relevance of the zebrafish CRISPant model, but also uncover new insights into the metabolic plasticity that may underlie tumor cell survival in the context of SDHB loss.

Because CRISPant models result in systemic gene disruption, we cannot formally attribute the observed phenotypes to specific tissues. However, given the strong and selective increase in catecholamines and MN observed in *sdhb* CRISPants, it is reasonable to assume that this hormonal dysregulation originates from the interrenal gland, the zebrafish homolog of the adrenal medulla. This interpretation is consistent with the known function and expression pattern of *sdhb* in endocrine tissues. Moreover, no tumors were observed in *sdhb*-CRISPant larvae (Fig. S2B, Fig. 2C), consistent with previous reports[17,23,24]. This is likely due to the limited lifespan of the model. Adrenal medullary hyperplasia may also occur in the absence of gross tumors and still be associated with catecholamine oversecretion[39]. While tissue-specific CRISPR knockouts would help refine tissue-level interpretation, the speed and scalability of the CRISPant approach enable rapid, large-scale functional screening. Future development of mosaic or conditional two-hit models will be important to more accurately mimic the clinical progression of *SDHB*-related PPGLs.

In conclusion, our zebrafish CRISPant model of SDHB loss recapitulates key features of human PPGLs, including elevated NM, succinate accumulation, mitochondrial reprogramming, and a distinct hypoxic/glycolytic transcriptional signature. This validates its utility as a physiologically relevant model for functional validation of PPGL genetic variants and opens new avenues for biomarker discovery and therapeutic screening in a high-throughput vertebrate system. By enabling rapid in vivo modeling of *SDHx* mutations, this platform could support precision medicine approaches in genetic pheochromocytoma and paraganglioma syndromes.

Methods

Zebrafish husbandry and euthanasia

Zebrafish (Danio rerio) larvae were maintained at 28 °C in E3 embryo medium under a 12 h/12 h light-dark cycle, following standard procedures described in *The Zebrafish Book*[40]. All experiments were approved by the Institutional Animal Care Committee of the CRCHUM (#F2PZ-85986) and conducted in compliance with the guidelines of the Canadian Council on Animal Care. Larvae were monitored daily and euthanized, when required, using an overdose of buffered tricaine methanesulfonate (MS-222) at a final concentration of 0.3% (w/v), followed by observation of cessation of heartbeat for at least 2 min before disposal. This method is consistent with the recommended practices for zebrafish euthanasia and was selected to minimize distress and ensure rapid and effective loss of consciousness.

Swim test

At 5 days post-fertilization (dpf), larvae were transferred individually into a 96-well plate and swim distance was recorded using Basler GenIcam infrared camera and DanioVision lightproof recording chamber with an infrared camera recording chamber (Noldus). Analysis was performed using the Ethovision XT 13 software (Noldus) to quantify the distance swam over time.

Zebrafish sdhb and nf1 CRISPant generation and scn1a genetic model

We designed gene-specific gRNA using the online tool CRISPRscan (http://www.crisprscan.org/). Three gRNAs were used against 3 exons of interest encoding important protein functional domains. For *sdhb*, we targeted exon 3 (GTCTGTTAGGTGTGGGCCGA), exon 4 (CAGCGTGTGTTGTGCTCCTC) and exon 5 (GGGCTCGATGGATTTATACT). For *nf1*, we targeted both zebrafish *nf1a* and *nf1b* paralogs on exons 17 (TTGGGTACGACTGTGTGAAC), exon 28 (GTAGGTAAACGTGCCTAGTA) and exon 36 (CGACTGCTGACTGGCCTCAA) for *nf1a* and exon 20 (CGGTCCAGAAAGCGGCCGAG), exon 25 (GCGAGGCATGTCCAGGCGAT) and exon 34 (GGGACCCAGGTAAGCGAGCA) for *nf1b*. The expression of *sdhb* is enriched in the brain and myotome, while *nf1a* and *nf1b* show broad expression, particularly in the head and heart[41,42].

Synthetic gRNAs were ordered from Synthego (CA, USA) and Cas9 mRNA was in vitro synthesized as described previously[43]. Zebrafish wild-type embryos were microinjected with a 1 nL drop of a mix of 100 ng/μL of Cas9 mRNA and 30 or 100 ng/μL of exon-specific gRNAs into one-cell stage embryos using a Picospritzer III pressure ejector. Control-injected embryos were microinjected following the same process but with Cas9 mRNA only (no gRNAs). As previously described, the mutagenic score of each gRNA was confirmed by HRM[44]. A stable genetic model of *scn1lab* (e.g. zebrafish ortholog of human *SCN1A*) with a frameshifting mutation (ins+1) in exon 8 (leading to a premature stop at position 288) was used as a model for Dravet syndrome a form of epileptic encephalopathy[45]. The identification of homozygous larvae was done via hyperpigmentation, as previously described[45]. Their siblings, which included healthy heterozygous and wild-type larvae, were taken as *+/sib* controls.

RT-qPCR and Western Blot

RT-qPCR was performed as previously described[46]. RNA was isolated from three sets of 5–7 larvae using QIAGEN Rneasy ® Plus Mini Kit according to the manufacturer's protocol. 500 ng of total RNA was used for cDNA synthesis using the SuperScript®Vilo™kit (Invitrogen). RT–qPCR was run with SYBR Green Master Mix (Bioline) using a LightCycler®96 (Roche). *Polr2d* was used as the reference gene for ddCt differential expression analysis. Primer sequences are available upon request. For western blot, whole proteins were extracted from pools of seven 5 dpf larvae using RIPA buffer supplemented with Protease Inhibitor Cocktail and PhosSTOP (Millipore Sigma). 50 μg of total proteins were immunoblotted using a monoclonal anti-SHDB antibody (1:1000, Abcam #ab14714; 5% milk in PBS Tween 0.1%) or a monoclonal anti-GAPDH antibody (1:500, Invitrogen MA5-44678; 5% BSA in PBS Tween 0.1%)). Relative expression analysis was performed using ImageLab software (Biorad).

Heart Rate Monitoring

5 dpf *sdhb*-mutant and *Cas9*-control zebrafish larvae were placed in a 6 cm plastic Petri dish. 3% methylcellulose was used to mount each larva laterally in order to see the heartbeat. No anesthetic (e.g., tricaine) was used during the procedure to avoid any confounding effects on cardiac activity. Video recordings of 1 min were captured for each fish group using an iPhone 6 and an ocular holder. Heart rate was quantified unbiasedly using the cardiology feature of the DanioScope™ software (Noldus).

Survival Assay

Groups of ~30 uninjected or injected larvae (either Cas9-control or *sdhb*-mutant) were raised in a 500 ml beaker, and they were fed every day from day 5. A mortality report was filled daily, and these values were plotted in a

Kaplan-Meier estimator, comparing mutant, Cas9-controls and wild-type larvae.

Targeted metabolomics

Pools of ten 4 dpf larvae (*sdhb*-CRISPant or Cas9-controls) were placed in 1.5 ml Eppendorf tubes with the lid open overnight at 28.5 °C. The following day (e.g., 5 dpf), the bathing medium (1 ml) was harvested and flash-frozen as well as dried larvae (pools of 10). Metabolites from central carbon metabolism were measured from pools of ten larvae as described previously[47] with the following modification: larvae pellets were extracted in ice-cold 80% methanol in water, 2 mM ammonium acetate, pH 9.0. Catecholamines were measured using a method modified from ref. 48. Briefly, samples of 10 larvae and 1 mL of bathing water were freeze-dried before addition of 30 µL of 80% acetonitrile in water, containing 50 nM of deuterated NM and norepinephrine as internal standards (CDN Isotopes, Pointe-Claire, QC, Canada). Larvae samples were sonicated in ice-cold water using a cup-horn sonicator (Q700, Qsonica, Newtown, CT) at 150 watts for 2 min (cycles of 10 s on, 10 s off). Both larvae and water samples were centrifuged 20,000 x g, 10 min at 4 °C. Supernatants (20 µL) were derivatized and analyzed as described in the original method. Detection of MN was achieved using transition 406.2/104.9 [M (with 2 benzoyl groups) + H +]. All quantitative results were normalized to the Cas9-control group.

RNA-sequencing

Total RNA was extracted from three batches of 5 dpf *sdhb*-CRISPant and Cas9-control larvae (10 larvae per sample). RIN greater than 9 was confirmed for each sample using an Agilent 2100 Bioanalyzer System. The NEBNext Ultra II directional RNA library prep kit for Illumina (New Englands Biolabs Inc., Ipswich, MA, USA) was used to prepare mRNA sequencing libraries, according to the manufacturer's instructions. Briefly, 1 ug of total RNA was purified using the NEBNext poly (A) mRNA Magnetic Isolation module (New England Biolabs Inc., Ipswich, MA, USA) and used as a template for cDNA synthesis by reverse transcriptase with random primers. The specificity of the strand was obtained by replacing dTTP with dUTP. This cDNA was subsequently converted to double-stranded DNA and end-repaired. Ligation of adapters was followed by a purification step with AxyPrep Mag PCR Clean-up kit (Axygen, Big Flats, NY, USA), by excision of the strands containing the dumps and finally, by a PCR enrichment step of nine cycles to incorporate specific indexed adapters for the multiplexing. The quality of final amplified libraries was examined with a DNA screentape D1000 on a TapeStation 2200, and the quantification was done on the QuBit 3.0 fluorometer (ThermoFisher Scientific, Canada). Subsequently, mRNA-seq libraries with unique dual indexes were pooled together in equimolar ratio and sequenced for paired-end 100 bp sequencing on an Illumina NovaSeq 6000 at the Next-Generation Sequencing Platform, Genomics Center, CHU de Québec-Université Laval Research Center, Québec City, Canada. The mean coverage/sample was 25 M paired-end reads.

Differential gene expression analysis

Alignment was performed using STAR in two pass mode (v2.7.11a) against the reference genome *Danio rerio* Ensembl version GRCz11.105. Read counts were obtained using featureCounts (v2.0.6) prior to DESeq2 (v1.42.1) differential expression quantification using R version 4.3.3. The Ensembl gene IDs were matched to gene names using biomaRt (v 2.58.2). Results (Supplementary Data 1) were filtered using an absolute log2 Fold Change ≥ 1 and p value of ≤ 0.05 for further gene ontology analysis. Data visualization was performed using several R packages. For PCA, the DEGs were transformed using the regularized log function and used in the pcaplot function of pcaExplorer (v1.0.2) using the top 1000 variables. Heatmaps were made using pheatmap (v1.0.12) and represent the top 20 most differentially expressed genes. The package ggplot2 (v 3.5.1) was used for volcano plots.

Oxygen consumption rate (OCR)

The day before the assay, Seahorse XF 96-well sensor cartridges (Agilent) were hydrated overnight at room temperature in the dark, using 200 µL of Seahorse XF calibrant (Agilent) per well. On the day of the assay, Cas9- or *sdhb*-injected zebrafish embryos were plated in a Seahorse XF 96-well cell culture microplate (Agilent) in a total volume of 200 µl of E3 medium.

The oxygen consumption rate (OCR) was measured during 25 cycles (mix: 0 min, wait: 1 min, measure: 2 min) using a Seahorse XFe96 analyzer (Agilent). The OCR data were analyzed using Wave 2.6.1 software (Agilent). The raw OCR data were first subjected to range-based filtering. Values falling outside the physiological range (< 30 or >400 pmol/min) were excluded as outliers. For each larva, we then computed the standard deviation (SD) of OCR measurements to evaluate signal consistency. Larvae were included in the analysis if the intra-individual SD was less than 50% of the mean OCR. For larvae exceeding this threshold, individual data points were examined, and a maximum of one outlier value was removed per larva. If this correction brought the SD below 50% of the mean, the larva was retained; otherwise, it was excluded from further analysis.

Statistical analysis

Graphpad Prism software (Version 9.5.1 for Mac, Graphpad Software, www.graphpad.com) was used to perform statistical analysis and generate graphs. T-tests were performed for variables following a normal distribution, while ANOVA was used for comparisons across multiple groups. For survival analysis, a Kaplan-Meier curve was generated, and statistical differences were assessed using a log-rank test.

Data availability

All data supporting the findings of this study are available within the paper and its Supplementary Information files. Raw sequencing data and raw counts matrix have been deposited in NCBI's Gene Expression Omnibus[49] and are accessible through GEO Series accession number GSE300914. Processed data, code used for data analysis, and additional datasets generated during the current study are available from the corresponding authors upon reasonable request.

Abbreviations

PPGLs	Pheochromocytomas and paragangliomas
PGLs	Paragangliomas
LCMS	liquid chromatography-mass spectrometry
gRNA	gene-specific guide RNAs
HRM	High-Resolution Melting

Received: 11 December 2024; Accepted: 22 July 2025;
Published online: 11 August 2025

References

1. Brewczynski, A., Kolasinska-Cwikla, A., Jablonska, B. & Wyrwicz, L. Pheochromocytomas and paragangliomas-current management. *Cancers* **17**, 1029 (2025).
2. Turchini, J., Cheung, V. K. Y., Tischler, A. S., De Krijger, R. R. & Gill, A. J. Pathology and genetics of phaeochromocytoma and paraganglioma. *Histopathology* **72**, 97–105 (2018).
3. Constantinescu, G. et al. Silent pheochromocytoma and paraganglioma: systematic review and proposed definitions for standardized terminology. *Front Endocrinol. (Lausanne)* **13**, 1021420 (2022).
4. Lenders, J. W. M. et al. Genetics, diagnosis, management and future directions of research of phaeochromocytoma and paraganglioma: a position statement and consensus of the Working Group on Endocrine Hypertension of the European Society of Hypertension. *J. Hypertens.* **38**, 1443–1456 (2020).
5. Jhawar, S. et al. New insights on the genetics of pheochromocytoma and paraganglioma and its clinical implications. *Cancers* **14**, 594 (2022).
6. Taïeb, D. et al. Management of phaeochromocytoma and paraganglioma in patients with germline SDHB pathogenic variants:

an international expert Consensus statement. *Nat. Rev. Endocrinol.* **20**, 168–184 (2024).
7. Crona, J., Taïeb, D. & Pacak, K. New perspectives on pheochromocytoma and paraganglioma: toward a molecular classification. *Endocr. Rev.* **38**, 489–515 (2017).
8. Nölting, S. et al. Personalized management of pheochromocytoma and paraganglioma. *Endocr. Rev.* **43**, 199–239 (2022).
9. Saavedra, T. J. et al. Pheochromocytoma: an updated scoping review from clinical presentation to management and treatment. *Front Endocrinol.***15**, 1433582 (2024).
10. Hamidi, O. et al. Malignant pheochromocytoma and paraganglioma: 272 patients over 55 years. *J. Clin. Endocrinol. Metab.* **102**, 3296–3305 (2017).
11. Lussey-Lepoutre, C., Pacak, K., Grossman, A., Taieb, D. & Amar, L. Overview of recent guidelines and consensus statements on initial screening and management of phaeochromocytoma and paraganglioma in SDHx pathogenic variant carriers and patients. *Best. Pr. Res. Clin. Endocrinol. Metab.* **39**, 101938 (2025).
12. Parasiliti-Caprino, M. et al. Predictors of recurrence of pheochromocytoma and paraganglioma: a multicenter study in Piedmont, Italy. *Hypertens. Res.* **43**, 500–510 (2020).
13. Johnston, P. C. et al. Recurrence of phaeochromocytoma and abdominal paraganglioma after initial surgical intervention. *Ulst. Med. J.* **84**, 102–106 (2015).
14. Parisien-La Salle, S. et al. Postoperative recurrences in patients operated for pheochromocytomas and paragangliomas: new data supporting lifelong surveillance. *Cancers* **14**, 2942 (2022).
15. Lenders, J. W. et al. Pheochromocytoma and paraganglioma: an endocrine society clinical practice guideline. *J. Clin. Endocrinol. Metab.* **99**, 1915–1942 (2014).
16. Davidoff, D. F. et al. Surveillance improves outcomes for carriers of SDHB pathogenic variants: a multicenter study. *J. Clin. Endocrinol. Metab.* **107**, e1907–e1916 (2022).
17. Lepoutre-Lussey, C. et al. From Nf1 to SDHB knockout: successes and failures in the quest for animal models of pheochromocytoma. *Mol. Cell Endocrinol.* **421**, 40–48 (2016).
18. Muth, A. et al. Genetic testing and surveillance guidelines in hereditary pheochromocytoma and paraganglioma. *J. Intern. Med.* **285**, 187–204 (2019).
19. Crona, J. et al. Genotype-phenotype correlations in pheochromocytoma and paraganglioma: a systematic review and individual patient meta-analysis. *Endocr. Relat. Cancer* **26**, 539–550 (2019).
20. Tabebi, M., Kumar Dutta, R., Skoglund, C., S"derkvist, P. & Gimm, O. Loss of SDHB induces a metabolic switch in the hPheo1 cell line toward enhanced OXPHOS. *Int. J. Mol. Sci* **23**, 560 (2022).
21. Fishbein, L. & Nathanson, K. L. Pheochromocytoma and paraganglioma: understanding the complexities of the genetic background. *Cancer Genet* **205**, 1–11 (2012).
22. Yang, C. et al. Missense mutations in the human SDHB gene increase protein degradation without altering intrinsic enzymatic function. *Faseb J.* **26**, 4506–4516 (2012).
23. Dona, M. et al. Loss of sdhb in zebrafish larvae recapitulates human paraganglioma characteristics. *Endocr. Relat. Cancer* **28**, 65–77 (2021).
24. Miltenburg, J. B. et al. Characterisation of an adult Zebrafish model for SDHB-associated phaeochromocytomas and paragangliomas. *Int. J. Mol. Sci.* **25**, 7262 (2024).
25. Kroll, F. et al. A simple and effective F0 knockout method for rapid screening of behaviour and other complex phenotypes. *Elife* **10**, e59683 (2021).
26. Mazeaud, M. M. & Mazeaud, F. Excretion and catabolism of catecholamines in fish. I. Excretion rates. *Comp. Gen. Pharm.* **4**, 183–187 (1973).
27. Braun, M. H., Steele, S. L., Ekker, M. & Perry, S. F. Nitrogen excretion in developing zebrafish (Danio rerio): a role for Rh proteins and urea transporters. *Am. J. Physiol. Ren. Physiol.* **296**, F994–F1005 (2009).
28. Tiraboschi, E. et al. New insights into the early mechanisms of epileptogenesis in a Zebrafish model of Dravet syndrome. *Epilepsia* **61**, 549–560 (2020).
29. Sherman, B. T. et al. DAVID: a web server for functional enrichment analysis and functional annotation of gene lists (2021 update). *Nucleic Acids Res.* **50**, W216–W221 (2022).
30. Alston, C. L. et al. Recessive germline SDHA and SDHB mutations causing leukodystrophy and isolated mitochondrial complex II deficiency. *J. Med. Genet.* **49**, 569–577 (2012).
31. Lamy, C. et al. Succinate: a serum biomarker of sdhb-mutated paragangliomas and pheochromocytomas. *J. Clin. Endocrinol. Metab.* **107**, 2801–2810 (2022).
32. Pang, Y. et al. Targeting NAD(+)/PARP DNA repair pathway as a novel therapeutic approach to SDHB-mutated cluster I pheochromocytoma and paraganglioma. *Clin. Cancer Res.* **24**, 3423–3432 (2018).
33. Hart, M. L. et al. Mitochondrial redox adaptations enable alternative aspartate synthesis in SDH-deficient cells. *Elife* **12**, e78654 (2023).
34. Yoo, H. C., Yu, Y. C., Sung, Y. & Han, J. M. Glutamine reliance in cell metabolism. *Exp. Mol. Med.* **52**, 1496–1516 (2020).
35. Saskői, É. et al. The SDHB Arg230His mutation causing familial paraganglioma alters glycolysis in a new Caenorhabditis elegans model. *Dis. Model Mech.* **13**, 44925 (2020).
36. Jochmanová, I., Yang, C., Zhuang, Z. & Pacak, K. Hypoxia-inducible factor signaling in pheochromocytoma: turning the rudder in the right direction. *J. Natl. Cancer Inst.* **105**, 1270–1283 (2013).
37. Selak, M. A. et al. Succinate links TCA cycle dysfunction to oncogenesis by inhibiting HIF-alpha prolyl hydroxylase. *Cancer Cell* **7**, 77–85 (2005).
38. Goncalves, J. et al. Loss of SDHB promotes dysregulated iron homeostasis, oxidative stress, and sensitivity to ascorbate. *Cancer Res.* **81**, 3480–3494 (2021).
39. Ganni, R., Torpy, D. J., Falhammar, H. & Louise Rushworth, R. Adrenal medullary hyperplasia: a systematic review and meta-analysis. *J. Clin. Endocrinol. Metab.* **108**, e885–e892 (2023).
40. Westerfield, M. The Zebrafish Book. A Guide for the Laboratory Use of Zebrafish (Danio rerio). *4th Edition (*University of Oregon Press, 2000).
41. Padmanabhan, A. et al. Cardiac and vascular functions of the zebrafish orthologues of the type I neurofibromatosis gene NFI. *Proc. Natl. Acad. Sci. USA* **106**, 22305–22310 (2009).
42. Bradford, Y. M. et al. Zebrafish information network, the knowledgebase for Danio rerio research. *Genetics* **220**, iyac016 (2022).
43. Moreno-Mateos, M. A. et al. CRISPRscan: designing highly efficient sgRNAs for CRISPR-Cas9 targeting in vivo. *Nat. Methods* **12**, 982–988 (2015).
44. Samarut, É., Lissouba, A. & Drapeau, P. A simplified method for identifying early CRISPR-induced indels in zebrafish embryos using high resolution melting analysis. *BMC Genomics* **17**, 547 (2016).
45. Baraban, S. C., Dinday, M. T. & Hortopan, G. A. Drug screening in Scn1a zebrafish mutant identifies clemizole as a potential Dravet syndrome treatment. *Nat. Commun.* **4**, 2410 (2013).
46. Jamadagni, P. et al. Chromatin remodeller CHD7 is required for GABAergic neuron development by promoting PAQR3 expression. *EMBO Rep.* **22**, e50958 (2021).
47. Mugabo, Y. et al. Metabolic fate of glucose and candidate signaling and excess-fuel detoxification pathways in pancreatic beta-cells. *J. Biol. Chem.* **292**, 7407–7422 (2017).
48. Wong, J. M. et al. Benzoyl chloride derivatization with liquid chromatography-mass spectrometry for targeted metabolomics of neurochemicals in biological samples. *J. Chromatogr. A* **1446**, 78–90 (2016).
49. Edgar, R., Domrachev, M. & Lash, A. E. Gene Expression Omnibus: NCBI gene expression and hybridization array data repository. *Nucleic Acids Res.* **30**, 207–210 (2002).

Acknowledgements
We thank the CRCHUM animal facility, particularly the zebrafish platform, for their help and support in maintaining our fish colonies. We also thank the Metabolomics Platform for their valuable support and contributions to this work. MT and ES are supported by the Fonds de Recherche du Québec en Santé (FRQS). SPL received grants Formation de recherche pour les résidents-Résidence complémentaire phase 1 FRQS and FMRQ (Fédération des médecins résidents du Québec). This work was supported in part by the Cancer Research Society (MT, IB). The Seahorse analyzer was acquired through a Young Investigator Infrastructure Grant from the Armand-Frappier Foundation and the Institut National de la Recherche Scientifique to LCC.

Author contributions
Conceptualization: S.P.L., I.B. and E.S.; Methodology: S.P.L., F.N., A.D.S.B., J.L., B.R., C.M., V.A.B.T. and G.C.; Investigation: S.P.L., I.B., and E.S.; Formal Analysis and Data Curation: S.P.L., F.N., A.D.S.B., J.L., M.L., M.T., I.B. and E.S.; Writing Original Draft: S.P.L., I.B. and E.S.; Writing – Review & Editing: M.D., M.T., I.B. and E.S.; Visualization: S.P.L. and E.S.; Supervision: L.C.C., M.T., I.B. and E.S.; Project Administration: I.B. and E.S.; Funding acquisition: I.B. and E.S.

Competing interests
The authors declare no competing interests.

Additional information
Supplementary information The online version contains supplementary material available at https://doi.org/10.1038/s41525-025-00518-z.

Correspondence and requests for materials should be addressed to I. Bourdeau or É. Samarut.